Hub GABA Neurons Mediate Gamma-Frequency Oscillations at Ictal-like Event Onset in the Immature Hippocampus

Pascale Quilichini, Michel Le van quyen, Anton Ivanov, Dennis Turner, Aurélie Carabalona, Henri Gozlan, Monique Esclapez, Christophe Bernard

Neuron 74, 57–64, April 12, 2012

Hub GABA Neurons Mediate Gamma-Frequency Oscillations at Ictal-like Event Onset in the Immature Hippocampus

Pascale P. Quilichini,[1,2,5] Michel Le Van Quyen,[3,5] Anton Ivanov,[1,2] Dennis A. Turner,[4] Aurélie Carabalona,[1,2] Henri Gozlan,[1,2] Monique Esclapez,[1,2,6] and Christophe Bernard[1,2,6,*]

[1]Institut de Neurosciences des Systèmes, INSERM UMR1106, Faculté de Médecine La Timone, 27 Boulevard Jean Moulin, 13005 Marseille, France
[2]Aix-Marseille Université, La Timone, 27 Boulevard Jean Moulin, 13005 Marseille, France
[3]Network Dynamics and Cellular Excitability, Centre de Recherche de l'Institut du Cerveau et de la Moelle Epinière, INSERM UMRS975, CNRS UMR7225, Université Pierre et Marie Curie, Hôpital de la Pitié-Salpêtrière, 47 Boulevard de l'Hôpital, 75651 Paris Cedex 13, France
[4]Duke University, DUMC 3807, Durham, NC 27710, USA
[5]These authors contributed equally to this work
[6]These authors contributed equally to this work

*Correspondence: christophe.bernard@univ-amu.fr

DOI 10.1016/j.neuron.2012.01.026

SUMMARY

Gamma-frequency oscillations (GFOs, >40 Hz) are a general network signature at seizure onset at all stages of development, with possible deleterious consequences in the immature brain. At early developmental stages, the simultaneous occurrence of GFOs in different brain regions suggests the existence of a long-ranging synchronizing mechanism at seizure onset. Here, we show that hippocamposeptal (HS) neurons, which are GABA long-range projection neurons, are mandatory to drive the firing of hippocampal interneurons in a high-frequency regime at the onset of epileptiform discharges in the intact, immature septohippocampal formation. The synchronized firing of interneurons in turn produces GFOs, which are abolished after the elimination of a small number of HS neurons. Because they provide the necessary fast conduit for pacing large neuronal populations and display intra- and extrahippocampal long-range projections, HS neurons appear to belong to the class of hub cells that play a crucial role in the synchronization of developing networks.

INTRODUCTION

The immature brain shows a higher susceptibility to epileptic seizures compared to the mature one (Holmes et al., 1998). Although there is more resistance to acute seizure-induced cell loss than in the adult brain, both clinical (Baram, 2003; Lombroso, 2007) and experimental (Holmes et al., 1998) studies have confirmed that frequent or prolonged seizures lead to long-term impairments in brain development and functional abnormalities. Transient gamma-frequency oscillations (GFOs; >40 Hz) occurring at the onset of most seizures are a marker of a chronic epileptic condition (Worrell et al., 2004). GFOs have been proposed to participate in the induction of alterations of immature networks (Khalilov et al., 2005). These GFOs occur simultaneously in different brain regions, suggesting a wide network-pacing system. Yet, the mechanisms underlying the emergence of GFOs and the control of their spatial synchronization are still unknown.

In adult networks, the mechanisms underlying GFO genesis involve synaptic interactions between glutamatergic and GABA neurons, as well as gap junctions (Bartos et al., 2007; Whittington and Traub, 2003). At early stages of postnatal development, pyramidal cells are poorly developed, and most function depends upon activation of GABA synapses (Ben-Ari et al., 1997). In this context, GFO mechanisms may differ from the adult situation and reflect the particular anatomical and functional organization of immature networks (Khalilov et al., 2005). Hence, our goal was to identify the cellular and network mechanisms underlying the generation and synchronization of GFOs in various conditions during development. We used the intact in vitro septohippocampal preparation, in which various stimuli can be used to trigger epileptiform discharges characterized by GFOs at their onset (Khalilov et al., 2005; Quilichini et al., 2002), thus enabling the study of their underlying mechanisms.

RESULTS

GFOs Occur Simultaneously in the Immature SHF at Seizure Onset

Field potential recordings performed in the intact septohippocampal formation (SHF) during the first postnatal (P) week (P5–7) in low Mg^{2+} conditions (Supplemental Experimental Procedures) revealed the presence of transient GFOs (peak frequency: 88 ± 6 Hz; duration: 143 ± 19 ms; n = 46 preparations) at the onset of regularly occurring ictal-like events (ILEs) (Quilichini et al., 2002) (Figures 1A and S1A, available online). GFOs were coordinated throughout the preparation: they occurred simultaneously and were phase locked in the different regions of the hippocampus and in the septum ($f_{DG}\, f_{CA1}$ = 13.8 ± 17.8; $f_{CA3}\, f_{CA1}$ = 85.4 ± 30.4; $f_{septum}\, f_{CA1}$ = 114.6 ± 31.5; n = 3; Figure 1B). There is thus a mechanism in the septohippocampal region that is able to transiently synchronize networks in the gamma-frequency range at the initiation of ILEs across quite large distances. Because this mechanism is at least present throughout CA1 (Figure S1B), it was further investigated in this region.

Interneurons Fire at High Frequency during GFOs, whereas HS Cells Fire before GFOs

Large populations of neurons fire action potentials during GFOs, thus contributing to the field activity (Chrobak and Buzsáki, 1996). We thus determined the firing pattern of different neuronal classes during GFOs. By using cell-attached recordings, we found that CA1 pyramidal cells (n = 10) were either silent (n = 8) or fired a single action potential (n = 2) during GFOs, and CA3 pyramidal cells (n = 10) fired at low rate (<25 Hz) (Figure 2A). Pyramidal cell always fired after GFO initiation (Figure 2A2). In contrast, all the CA1 interneurons recorded (n = 36; Figure S2), including basket cells (n = 3), O-

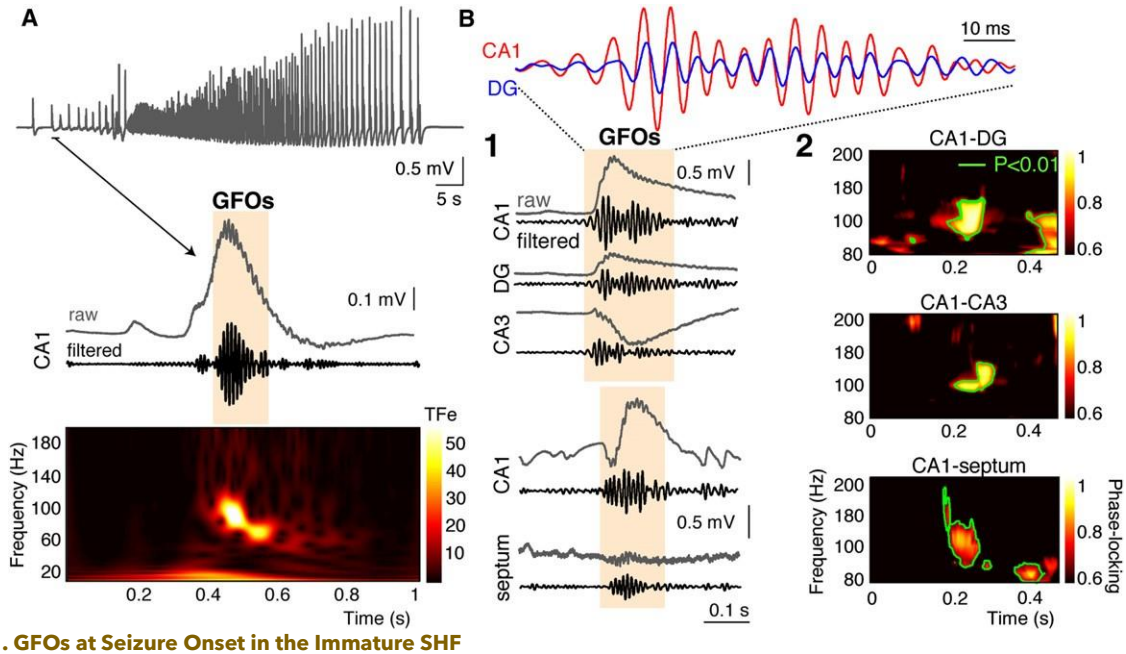

Figure 1. GFOs at Seizure Onset in the Immature SHF

(A) ILE recorded extracellularly in the CA1 area of a P7 SHF expresses GFOs at its onset, as evidenced by 60–120 Hz band-pass filtering and by the timefrequency (TF) representation (TFe: TF energy, color coded in standard deviations above the mean power of an event-free baseline). (B1) GFOs occur simultaneously in the dentate gyrus (DG) and in the CA3 and CA1 regions, as well as between the septum and the CA1 region. (B2) TF analysis of phase locking between the different regions of the SHF reveals a significant enhancement of phase synchrony around 100 Hz (green contour line: $p < 0.01$).

LM cells (n = 7), and backprojecting cells (n = 4), fired at high frequency exclusively during GFOs, reaching a maximum firing rate of 72 ± 10 Hz (range: 40–100 Hz), i.e., at nearly the same frequency as GFOs (Figure 2B1). Before GFO occurrence, all GABA neurons, except hippocamposeptal (HS) cells, described below, had a low-firing rate (2 ± 2 Hz; range: 0–9 Hz; n = 36), and the transition to high-firing rate during GFOs was abrupt (Figure 2A2). Moreover, their action potentials were phase locked to GFOs, arising preferentially at the descending phase of each cycle (34.4 ± 80; R = 0.35; p < 0.001; Rayleigh test; Figure 2B2). These results are in agreement with the initial assumption that interneurons are the main contributors to GFO generation. Accordingly, we found that GFOs depend upon $GABA_A$, but not AMPA, receptor activation (Figure S1C).

One type of GABA neuron, the HS cells, showed a different firing pattern. They always fired before GFO onset, with a 10–300 ms time lag (69 ± 35 ms; n = 23), reaching a maximal peak frequency of 96 ± 25 Hz (Figure 3A). These neurons belonged to the class of long-range projection GABA neurons (Figure 3A2) (Gulyás et al., 2003). Morphological analysis revealed that HS cells, although still in an early developmental stage, exhibited an extensive axon arborization in the different CA1 layers along the septotemporal axis, as well as in the septum (Figure 3A2). During development, they are known to contact GABA neurons exclusively (Gulyás et al., 2003). Because of their early firing, we reasoned that HS cells might have a pivotal role in GFO emergence by synchronizing their target interneurons (i.e., GABA neurons with exclusive local projections) into high-frequency firing, thus generating field GFOs. The firing patterns of the different cell types during GFOs are consistent with this hypothesis. If HS cells play a leading role in synchronizing their targets, we propose the following scheme: (1) a progressive recruitment of HS cells, because transient network events may involve a progressive recruitment of leading cells (de la Prida et al., 2006); (2) a depolarizing action of GABA onto interneurons; and (3) a recruitment of the interneurons (with exclusive local projections) by the HS cells. Finally, if a causal link exists between HS firing and GFO emergence, preventing HS cell firing should abolish GFOs. We directly tested these proposals.

HS Cells Orchestrate the Synchronization of Hippocampal Interneurons during GFOs

We first investigated the possibility of a buildup mechanism among interconnected HS cells. We analyzed the firing behavior of eleven HS cell pairs (four reciprocal and seven unidirectional connections; Figures S3A and S3B). Before GFO genesis, HS cell firing started to accelerate at a mean instantaneous frequency of 28 ± 11 Hz until an abrupt transition to highfrequency firing occurred within 150 ± 65 ms before GFO onset (Figure 3B). In keeping with a progressive recruitment of HS cells, there was a regular increase in GABAergic currents received by both HS cells and interneurons (Figure 3B3). Dual recordings revealed that HS cells were connected together and to other GABA neurons (four unidirectional HS to O-LM connections, three HS to O-LM reciprocal connections; Figures S3A and S3B). During the buildup process, the frequency of GABA currents remained low, consistent with the low-frequency firing of HS cells before their transition to high-frequency firing (Figure 3B3). The switch to high-frequency firing of HS cells correlated with the high-frequency GABA currents received by the interneurons (Figure 3B3). Those results are thus in favor of a progressive recruitment of HS cells.

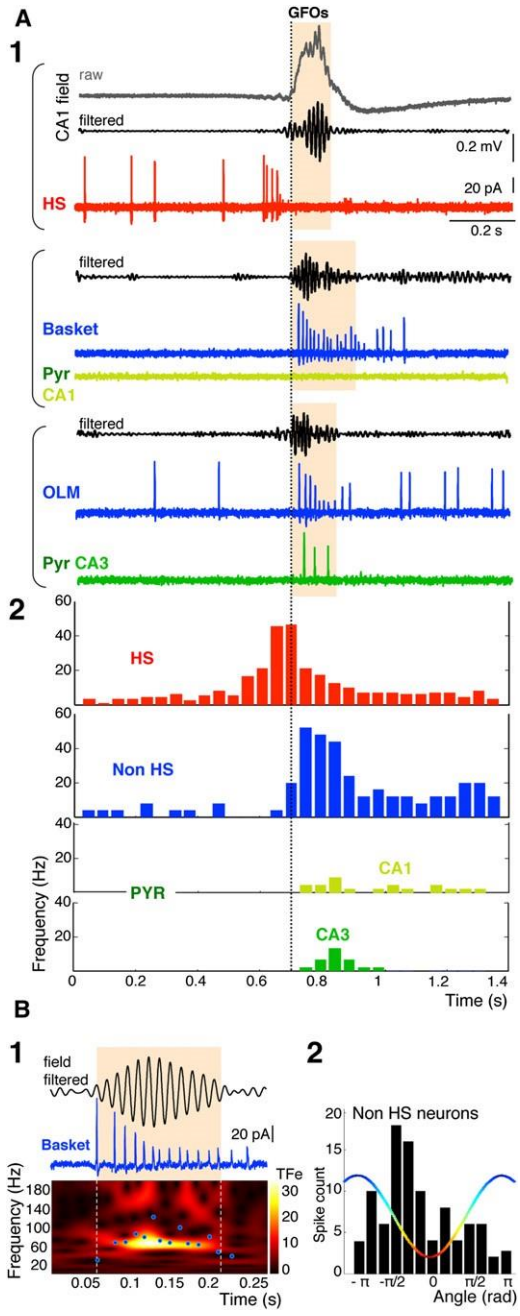

Figure 2. Interneurons Fire during GFOs

(A1) Firing patterns of simultaneously (bracket) recorded neurons (HS, basket, O-LM, CA1, and CA3 pyramidal cells and cell-attached recording; see Figure S2 for the morphology of the identified neurons) in three different experiments. The traces are aligned at the onset of each GFO episode. After GFO onset, interneurons fire at high frequency, whereas pyramidal cells either are silent or fire at a lower frequency. (A2) Mean firing activity of HS cells (n = 23), interneurons (n = 36), CA3 (n = 10), and CA1 (n = 10) pyramidal cells; bin size: 40 ms. (B1) The instantaneous firing frequency of a basket cell (blue dots) is plotted against the GFO TF plot. The neuron firing follows the GFO frequency. (B2) Interneurons (n = 36) fire preferentially during the descending phase of the GFO cycle.

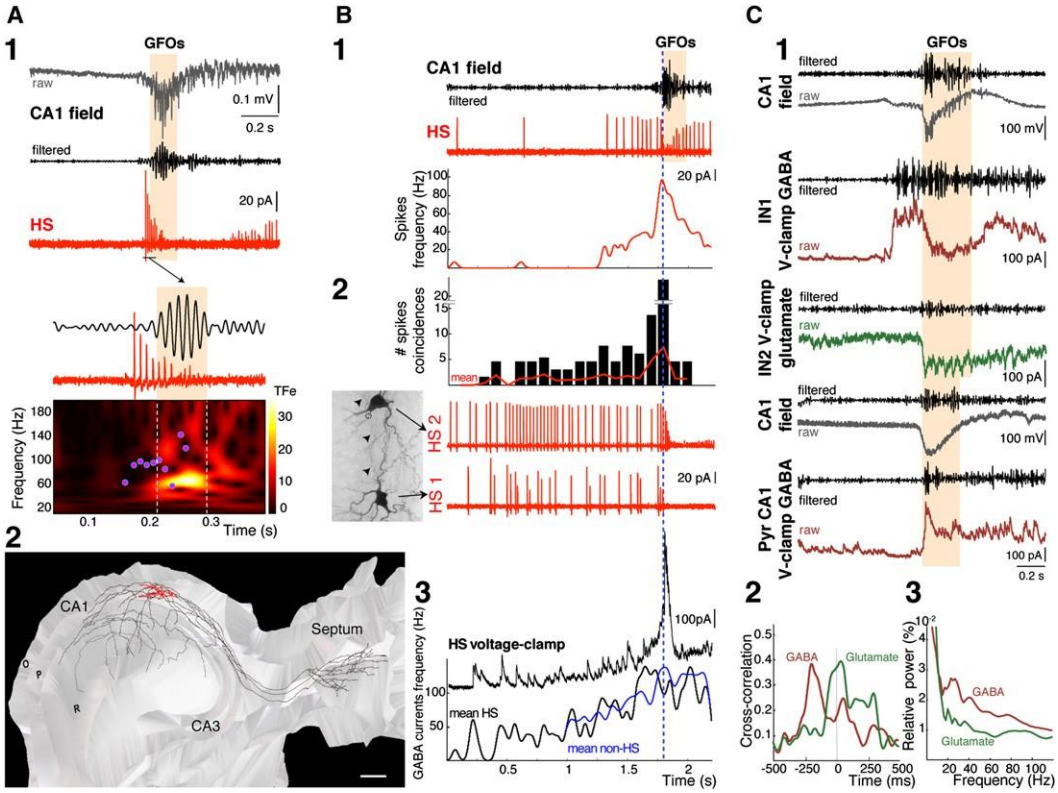

Figure 3. HS Neuron Firing Precedes Field GFOs

(A1) The HS cell high-frequency firing (cell-attached recording) precedes the GFOs. The decrease in spike amplitude during the burst is probably due to the inactivation of Na+ channels. Its instantaneous firing frequency (pink dots) is plotted against the GFO TF plot. (A2) Three-dimensional reconstruction of an HS cell is depicted. The soma (red) of the HS cell is located in stratum oriens and displays horizontally running dendrites (red). The axon (black) gives rise to many collaterals invading the septum, as well as all layers of the CA1 hippocampal region along the septotemporal axis. O, stratum oriens; P, stratum pyramidale; R, stratum radiatum. Scale bar represents 200 mm. (B1) The progressive increase in the HS cell firing (top: cell-attached recording; bottom: instantaneous spike frequency) before GFO onset suggests a buildup process. (B2) Increased degree of spike coincidences (within 15 ms; n = 3) before GFOs in simultaneous recording of two connected HS cells (HS1 and HS2; cell-attached configuration). Morphological recovery of the pair of HS cells shows a putative synaptic contact (dotted circle) between the axon (arrowheads) of the HS cell 1 and one dendrite of the HS cell 2. (B3) A progressive increase in the frequency of GABA postsynaptic currents in an HS cell can be seen 10–300 ms before GFOs, as evidenced by mean instantaneous frequency of GABA currents received by HS cells (n = 8) and interneurons (n = 22). (C1) Synaptic currents recorded in different O-LM interneurons (IN1 and IN2) and a CA1 pyramidal cell at holding potentials of +10mV (GABA currents) and –60mV (AMPA and NMDA receptor-mediated currents). Interneurons were recorded simultaneously during GFOs. The pyramidal cell was recorded later in the same preparation. The traces are aligned on GFO onset. In interneurons, but not in pyramidal cells, GABA currents containing gamma-frequency components (40–120 Hz filtered) precede the GFOs by several hundreds of ms. (C2) Mean crosscorrelation between GABA currents or glutamatergic currents and the corresponding GFOs for several interneurons (n = 17). Note the significant peaks, around 200 ms, in the GABA/field correlation. (C3) High-frequency components (20–90 Hz) predominate in GABA currents over glutamatergic currents in interneurons (n = 8) during GFOs.

We then analyzed the nature of the neurotransmission between HS cells and their targets in normal artificial cerebrospinal fluid (four reciprocal and seven unidirectional HS pairs, four unidirectional HS to O-LM connections, three HS to O-LM reciprocal connections; Figure S3A and S3B). The neurotransmission was extremely reliable at these synapses (1.0 release probability; n = 25 connections). Intracellular chloride concentration increases in epileptic conditions in the immature brain, rendering GABA strongly excitatory (Dzhala et al., 2010). By using noninvasive measurements of the resting membrane potential and the reversal potential of chloride in different classes of GABA neurons, we found that E_{Cl} was 19.1mV ± 1.9mV (n = 6 HS cells, 3 O-LM cells, 1 basket cell, and 2 unidentified interneurons; Figures S3C and S3D) above resting membrane potential (69.7mV ± 2.8mV; n = 12), indicating a depolarizing action of GABA. We also found that high-frequency stimulation of HS cells evoked action potentials in their target cells (n = 5 SHFs; Figure S3E2b). These results show that HS cell firing can entrain their target neurons, probably via the depolarizing action of GABA.

Our next proposal was a recruitment of interneurons by the HS cells. If HS firing entrained these interneurons, then two requirements should be met: (1) high-frequency GABA currents should occur in interneurons before GFOs, because HS cells, which contact interneurons, always fire before GFOs at high frequency; and (2) high-frequency GABA currents should occur in turn after GFO onset in pyramidal cells, because interneurons, which contact pyramidal cells, fire at high frequency during GFOs. Whole-cell recordings of interneurons revealed that large synaptic GABA currents with a high-frequency component always preceded field GFOs (mean: 183 ms; range: 40– 450 ms; n = 17; Figure 3C). Because pyramidal cell-projecting interneurons fire at high frequency during GFOs (Figure 2A), pyramidal cells received a high-frequency barrage of GABAergic inputs during GFOs (Figure 3C). The frequency of GABAergic inputs in pyramidal cells (88 ± 17 Hz; n = 9) was similar to the firing frequency of interneurons and to the field

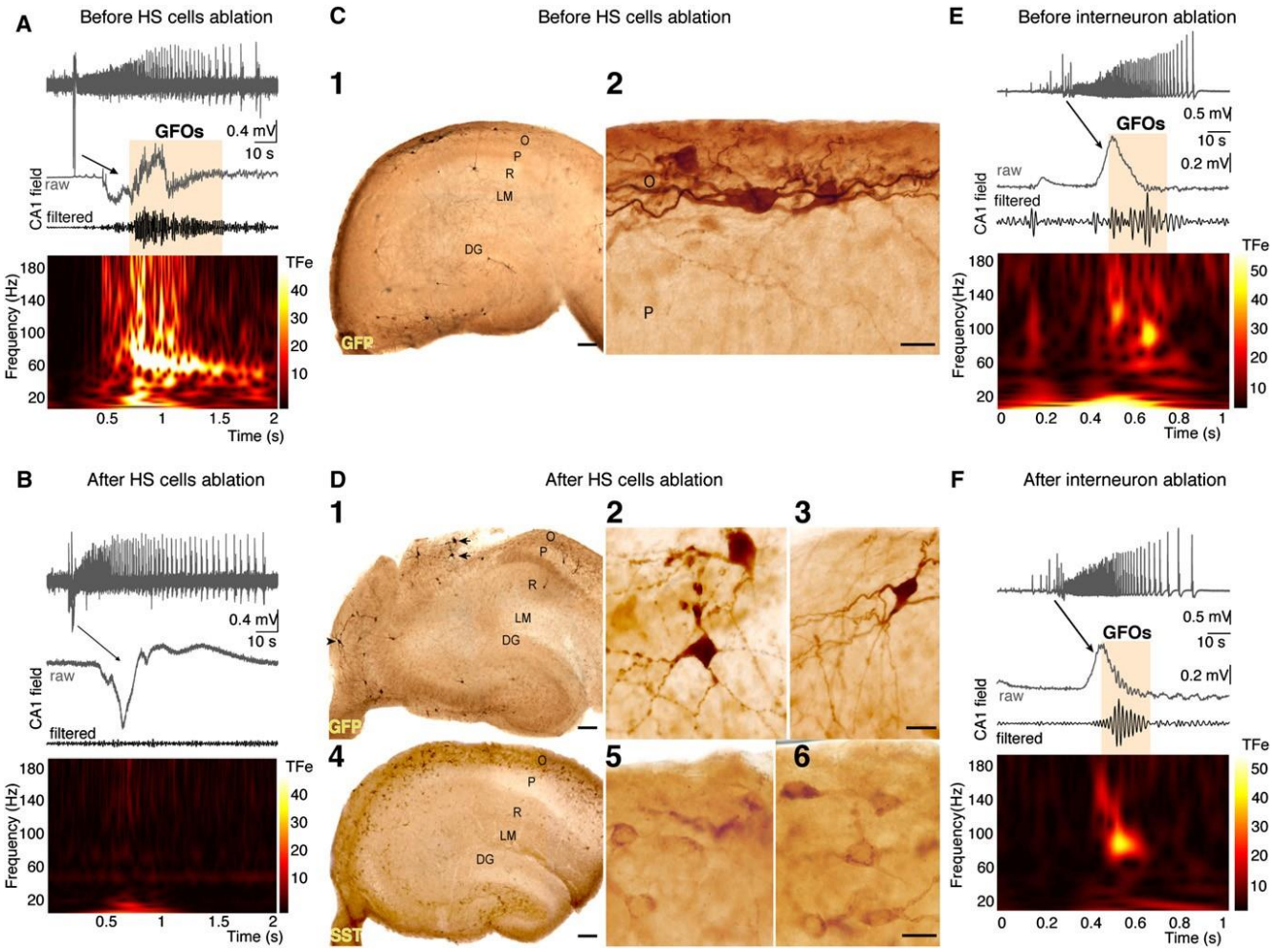

Figure 4. GFOs Are Abolished by the Elimination of HS Cells

(A) GFOs recorded in the CA1 region of the SHF of GIN mice at P6 before targeted illumination. (B) Specific elimination of GFP-positive GABA neurons by focused fluorescence illumination of the stratum oriens (SO) abolishes GFOs without affecting the occurrence of network discharges. ILEs recorded before and after illumination are similar, with tonic-clonic and clonic phases. (C1) Distribution of GFP-positive GABA neurons in a hippocampal section of the GIN mice SHF used for electrophysiological recordings after sham fluorescence illumination. (C2) Note the presence of healthy-appearing putative HS cells. (D) Two consecutive sections show the distribution of GFP-containing (D1–D3) and somatostatin-containing (D4–D6) neurons in GIN mice SHFs after focused SO fluorescence illumination and electrophysiological recordings. (D1–D3) In the close vicinity of the illuminated regions (D1), GFP-containing neurons (arrows) display typical features of suffering neurons, including beaded dendrites (D2). In contrast, GFP-containing neurons (D3; arrowhead in D1) located well outside (>500 mm) the illuminated area show healthy-like dendritic and axonal arborizations. (D4–D6) Both in the directly illuminated and nonilluminated regions, somatostatincontaining neurons can be clearly identified. This suggests that GFP-positive neurons were destroyed in the fluorescence-illuminated region, whereas GFPnegative neurons in the same illuminated area were preserved. (D4) Outside this area, the cytoarchitecture is mostly preserved. Scale bars represent 100 mm in (C1), (D1), and (D4) and 25 mm in (C2), (D2), (D3), (D5), and (D6). (E) GFOs recorded in the CA1 region of the SHF of GIN mice at P6 before GFP-negative neurons' ablation. (F) Elimination of 50 GFP-negative interneurons did not modify the expression of GFOs or the occurrence of ILEs.

GFOs. In contrast, the fast oscillatory component within the glutamatergic drive occurred after the initiation of GFOs in all recorded interneurons (n = 17) and pyramidal cells (n = 9) and had a lower magnitude than GABA currents (Figures 3C2 and 3C3). The analysis of synaptic activity thus reveals a sequential recruitment of the different actors in the network: at first, a population of GABA neurons (interneuron-specific GABA neurons), which contact interneurons, but not pyramidal cells, starts to fire before GFOs. This is consistent with the HS cells' specific targeting and firing pattern. This suggests that GABAergic currents provide the main synaptic drive onto interneurons. In turn, these interneurons fire during GFOs. Pyramidal cells also fire during GFOs, although to a lesser extent.

HS Cells Are Mandatory for GFO Emergence, but Not to Seizure

If HS cells play a leading role and are necessary for GFO emergence, preventing their firing should abolish GFOs. To test causality, we used GIN (GFP-expressing inhibitory neurons) mice in which green fluorescent protein (GFP) is expressed via the GAD67 promoter only in somatostatin-containing neurons, including HS cells (Oliva et al., 2000). At P6, most GFP-containing neurons recorded in CA1 stratum oriens were identified post hoc as HS cells (72%; n = 18/25). The 28% that remained were all identified as O-LM cells (n = 7/25). Recordings of GFP-negative interneurons revealed the presence of O-LM cells, but not HS cells (n = 14 O-LM cells and

14 other types of interneurons; data not shown). This suggests that the vast majority of GFP-containing neurons in CA1 stratum oriens at P6 are HS cells (Figure S4A) and that many O-LM cells do not express GFP at this age. GFOs, cell-firing patterns, and synaptic inputs in GIN mice had properties similar to those found in rats (Figures 4A and S4B). We also used this preparation to test other models of acute seizures: high K^+, kainic acid, and 4-AP. In all three models, GFOs (96 ± 7 Hz; range: 40–180 Hz; n = 22) were present at seizure onset, HS cells (115 ± 14 Hz; range: 40–208 Hz; n = 13) started to fire before the GFOs (mean time lag: 105 ± 19 ms), and the interneurons generated spikes only during the GFOs (81 ± 11 Hz; range: 34–117 Hz; n = 9, including 8 OLM cells and 1 backprojecting cell; Figures S4C–S4E). Whole-cell recordings of interneurons also showed large GABA synaptic currents preceding GFOs (102 ± 31 ms; range: 35–210 ms; n = 5; data not shown). These features are similar to the ones obtained in low Mg^{2+} conditions, demonstrating the generality of the mechanism involved in triggering GFOs at ILE onset at this stage of development.

Because the disappearance of a critical number of long-range projection neurons disrupts long-range synchrony (DyhrfjeldJohnsen et al., 2007), we eliminated stratum oriens GFP-positive cells successively along the septotemporal axis by using focused fluorescence illumination (Figure 4D; n = 8 SHFs). The elimination of between 10 and 20 GFP-positive cells (n = 8 SHFs) was sufficient to abolish GFOs without affecting the occurrence of ILEs (Figures 4A and 4B). The network structure and function did not appear damaged by this procedure: GFPnegative cells within the illuminated area and GFP-positive cells outside the illuminated area did not display apparent morphological damage (Figure 4D), and ILEs were still present (Figure 4B). The disappearance of GFOs could result from the loss of the trigger (HS cells) and/or the generator (interneurons). Because only a fraction of O-LM cells (GFP positive) were removed from the circuitry, and all the other generators (including GFP-negative O-LM and basket cells) were not affected, GFO disappearance most likely results from the loss of a critical mass of HS cells (Figure 4D). Accordingly, the elimination of up to 50 GFP-negative interneurons (n = 4 SHFs) did not affect the occurrence of GFOs at ILE onset (Figures 4E and 4F). Finally, while recording from pairs of HS cells, we generated simultaneous trains of action potentials at 100 Hz in each pair. This was not sufficient to entrain the system to produce field GFOs, in keeping with the proposal that a critical mass of HS cells needs to be recruited.

DISCUSSION

In this study, we have shown in the immature SHF that (1) field GFOs are present at ILE onset; (2) long-range projection HS cells start to fire at high frequency before field GFOs; (3) all the interneuron types recorded fire in turn high-frequency action potentials arising preferentially at the descending phase of the GFOs; and (4) GFOs are abolished after the elimination of a small number of HS cells. Taken together, we propose that HS cells, via their target-selective excitatory GABA synapses and their extensive axonal projections, provide the necessary fast conduit for synchronizing the hippocampal interneurons into transient high-frequency firing, leading to GFO emergence at the onset of epileptiform discharges.

The mechanisms that underlie GFOs in epileptogenic conditions at early stages of development contrast with those arising in physiological conditions. Several observations suggest that spontaneous GFOs are not present in developing networks. In rat pups, high-frequency (120–180 Hz) oscillations are observed in vivo in the hippocampus after the end of the second postnatal week (Buhl and Buzsáki, 2005). Moreover, various in vitro GFOgenerating procedures or agents, such as bath application of the ACh receptor agonist carbachol of intact cortex of newborn rats (Kilb and Luhmann, 2003) or high-frequency stimulation of CA1 afferents in rat hippocampal slices (Ruusuvuori et al., 2004), failed to generate GFOs during the first postnatal week. Because physiological GFOs are largely driven by glutamate in mature networks (Bartos et al., 2007; Fisahn et al., 1998; Traub et al., 1998; Whittington and Traub, 2003), these observations are consistent with the delayed maturation of glutamatergic synapses shown in a wide range of brain structures (Gozlan and Ben-Ari, 2003). As suggested previously (Traub et al., 1998), developing networks would lack the critical density of functional glutamatergic synapses required for these oscillatory activities. However, GFOs can emerge in epileptogenic conditions, signaling a pathological state. We showed that AMPA receptor activation is not necessary for GFO expression, and the glutamatergic drive always follows the GABAergic one in all neuron types. This is also consistent with other findings showing that synchronization of GABA neurons can occur in the absence of fast glutamatergic signaling via depolarizing GABA (Avoli and Perreault, 1987; Michelson and Wong, 1991). Furthermore, this is also in agreement with the tetanic model of GFOs that displays comparable GABA mechanisms to the low Mg^{2+} model (Fujiwara-Tsukamoto et al., 2006), because it also requires a depolarizing GABA action (Ko¨ hling et al., 2000), which is due to intracellular chloride accumulation during recurrent seizures (Dzhala et al., 2010).

Although very high-frequency oscillations (HFOs in the ripples: 140–200 Hz; fast ripples: 200–500 Hz) can be recorded in adult epileptic networks in vitro (Khosravani et al., 2005; Traub et al., 2001) and in vivo (Jirsch et al., 2006), the GFOs recorded in our conditions never reached such frequencies during the first postnatal week, probably reflecting the immature stage of development (Buhl and Buzsáki, 2005). It has been suggested that recurrent glutamatergic synaptic transmission (Dzhala and Staley, 2004) and pyramidal axoaxonic gap junctions (Traub et al., 2002) are instrumental in the generation of HFOs in the adult brain. This implies that these additional mechanisms are not yet fully functional. Nevertheless, the immature hippocampus has already reached a sufficient level of organization to generate GFOs (40–100 Hz) under epileptogenic conditions.

Collectively, our results provide strong support for the concept that, in different epileptogenic conditions at early stages of development, long-range projection neurons can trigger the high-frequency firing of interneurons with exclusive local connectivity, which leads to the emergence of GFOs. Although most of HS cells continued to fire at high frequency during GFOs, thus contributing to their expression, their main impact appears to be in coordinating the activity of their targets. In the adult brain, long-range projection neurons, which can contact both pyramidal cells and interneurons (Jinno et al., 2007; Takács et al., 2008), may fulfill the role of synchronizing elements (Tort et al., 2007). In our conditions, HS cells do not

appear to functionally contact pyramidal cells, because GABAergic currents should have occurred simultaneously in pyramidal cells and interneurons. Whether this discrepancy reflects a maturation process of these neurons and/or the existence of different classes of long-range projection neurons (Jinno et al., 2007) remains to be determined.

Interestingly, GFP expression in GIN mice is driven via the GAD67 promoter. GAD67 expression is developmentally regulated and is lower at the end of the first postnatal week as compared to adults (Jiang et al., 2001). Hence, at P6, GFPnegative neurons might include immature somatostatin-containing neurons (in which GAD67 expression is still low and would increase later in development) in addition to SST-negative neurons. This also suggests that HS cells, which form the vast majority of GFP-positive neurons, already display at P6 features of mature neurons, as compared to other future somatostatincontaining interneurons. We show here that these long-range projection neurons play a key role in triggering network synchronization and GFO expression. Interestingly, some ''connector hub neurons'' described in immature mouse hippocampal slices also show an extended axonal arborization (within the hippocampus), a similar coactivation (built up of synchronization) before the onset of network activity (giant depolarizing potentials), and orchestration of spontaneous network synchronization (Bonifazi et al., 2009). Besides, early-generated GABA hub neurons preferentially express somatostatin and were recently proposed to develop into GABA projection neurons (Picardo et al., 2011). It has also been suggested that GABA neurons displaying long-range axonal arborization which extends the outside of the hippocampus would carry such a hub function and would support the emergence of network oscillations (Buzsáki et al., 2004). Thus, HS cells are likely to belong to this class of hub neurons and to form such a hub network that is critical for broad network synchronization during development. In keeping with such an assumption, the elimination of some HS cells abolished GFOs, but not the ILEs themselves.

Altogether, our results have two major implications. (1) In contrast to adult networks (Jirsch et al., 2006; Steriade and Demetrescu, 1966) and with the caveat that we used an in vitro acute model of epilepsy, we propose that GFOs may not be causally linked to seizure genesis at early stages of development. They would sign the activity of a network before its transition to the ictal discharge. (2) Few hub-like GABA neurons, i.e., HS cells, are able to synchronize wide-reaching, large neuronal populations that enable GFOs to emerge, a phenomenon that may also be valid in physiological conditions.

EXPERIMENTAL PROCEDURES

Intact septohippocampal formations were prepared from 5- to 7-day-old rats and GIN mice. Extracellular, cell-attached, and voltage-clamp whole-cell recordings were performed at 33C from hippocampal CA1 pyramidal cells and interneurons. GFOs were quantified using wavelet time-frequency analysis. GABAergic and glutamatergic synaptic currents were measured at +10mV and 60mV, respectively. Resting membrane potential and the reversal potential of GABAergic currents were measured using single NMDA and $GABA_A$ receptor-channel recordings in the cell-attached configuration. Synaptic connections between cells were determined by making one cell fire an action potential and by detecting the presence of a postsynaptic GABA current in the second cell. Ablation of GFP-containing neurons was obtained after 5-min-long high-power fluorescence focused through a 603 objective. All recorded cells were filled with biocytin for post hoc morphological identification. They were reconstructed using the Neurolucida system. Immunohistochemical labelings for GFP- and somatostatin-containing neurons were performed by using polyclonal antisera directed against GFP and somatostatin, respectively.

SUPPLEMENTAL INFORMATION

Supplemental Information includes four figures and Supplemental Experimental Procedures and can be found with this article online at doi:10.1016/ j.neuron.2012.01.026.

ACKNOWLEDGMENTS

This work was supported by INSERM, Fondation pour la Recherche sur le Cerveau, Fédération Française de la Recherche sur l'Epilepsie, Fondation pour la Recherche Médicale (P.P.Q.), Ligue Française Contre l'Epilepsie (P.P.Q.), NIH (F33NS062617 to D.A.T. and C.B.), The Philippe Foundation (D.A.T.), and the Letten Foundation (C.B.). Initial experiments were performed in Y. Ben-Ari's laboratory (INMED-INSERM U29). We thank G. Buzsáki and D. Johnston for helpful comments on the manuscript, and M. Fontes for hosting A.C., M.E., and C.B. in his laboratory.

Accepted: January 18, 2012
Published: April 11, 2012

REFERENCES

Avoli, M., and Perreault, P. (1987). A GABAergic depolarizing potential in the hippocampus disclosed by the convulsant 4-aminopyridine. Brain Res. 400, 191–195.

Baram, T.Z. (2003). Long-term neuroplasticity and functional consequences of single versus recurrent early-life seizures. Ann. Neurol. 54, 701–705.

Bartos, M., Vida, I., and Jonas, P. (2007). Synaptic mechanisms of synchronized gamma oscillations in inhibitory interneuron networks. Nat. Rev. Neurosci. 8, 45–56.

Ben-Ari, Y., Khazipov, R., Leinekugel, X., Caillard, O., and Gaiarsa, J.L. (1997). GABAA, NMDA and AMPA receptors: a developmentally regulated 'mé nage a` trois'. Trends Neurosci. 20, 523–529.

Bonifazi, P., Goldin, M., Picardo, M.A., Jorquera, I., Cattani, A., Bianconi, G., Represa, A., Ben-Ari, Y., and Cossart, R. (2009). GABAergic hub neurons orchestrate synchrony in developing hippocampal networks. Science 326, 1419–1424.

Buhl, D.L., and Buzsáki, G. (2005). Developmental emergence of hippocampal fast-field ''ripple'' oscillations in the behaving rat pups. Neuroscience 134, 1423–1430.

Buzsáki, G., Geisler, C., Henze, D.A., and Wang, X.J. (2004). Interneuron Diversity series: Circuit complexity and axon wiring economy of cortical interneurons. Trends Neurosci. 27, 186–193.

Chrobak, J.J., and Buzsáki, G. (1996). High-frequency oscillations in the output networks of the hippocampal-entorhinal axis of the freely behaving rat. J. Neurosci. 16, 3056–3066.

de la Prida, L.M., Huberfeld, G., Cohen, I., and Miles, R. (2006). Threshold behavior in the initiation of hippocampal population bursts. Neuron 49, 131–142.

Dyhrfjeld-Johnsen, J., Santhakumar, V., Morgan, R.J., Huerta, R., Tsimring, L., and Soltesz, I. (2007). Topological determinants of epileptogenesis in largescale structural and functional models of the dentate gyrus derived from experimental data. J. Neurophysiol. 97, 1566–1587.

Dzhala, V.I., and Staley, K.J. (2004). Mechanisms of fast ripples in the hippocampus. J. Neurosci. 24, 8896–8906.

Dzhala, V.I., Kuchibhotla, K.V., Glykys, J.C., Kahle, K.T., Swiercz, W.B., Feng, G., Kuner, T., Augustine, G.J., Bacskai, B.J., and Staley, K.J. (2010). Progressive NKCC1-dependent neuronal chloride accumulation during neonatal seizures. J. Neurosci. 30, 11745–11761.

Fisahn, A., Pike, F.G., Buhl, E.H., and Paulsen, O. (1998). Cholinergic induction of network oscillations at 40 Hz in the hippocampus in vitro. Nature 394, 186–189.

Fujiwara-Tsukamoto, Y., Isomura, Y., and Takada, M. (2006). Comparable GABAergic mechanisms of hippocampal seizurelike activity in posttetanic and low-Mg2+ conditions. J. Neurophysiol. 95, 2013–2019.

Gozlan, H., and Ben-Ari, Y. (2003). Interneurons are the source and the targets of the first synapses formed in the rat developing hippocampal circuit. Cereb.
Cortex 13, 684–692.

Gulyás, A.I., Hájos, N., Katona, I., and Freund, T.F. (2003). Interneurons are the local targets of hippocampal inhibitory cells which project to the medial septum. Eur. J. Neurosci. 17, 1861–1872.

Holmes, G.L., Gairsa, J.L., Chevassus-Au-Louis, N., and Ben-Ari, Y. (1998). Consequences of neonatal seizures in the rat: morphological and behavioral effects. Ann. Neurol. 44, 845–857.

Jiang, M., Oliva, A.A., Jr., Lam, T., and Swann, J.W. (2001). GABAergic neurons that pioneer hippocampal area CA1 of the mouse: morphologic features and multiple fates. J. Comp. Neurol. 439, 176–192.

Jinno, S., Klausberger, T., Marton, L.F., Dalezios, Y., Roberts, J.D., Fuentealba, P., Bushong, E.A., Henze, D., Buzsáki, G., and Somogyi, P. (2007). Neuronal diversity in GABAergic long-range projections from the hippocampus. J. Neurosci. 27, 8790–8804.

Jirsch, J.D., Urrestarazu, E., LeVan, P., Olivier, A., Dubeau, F., and Gotman, J. (2006). High-frequency oscillations during human focal seizures. Brain 129, 1593–1608.

Khalilov, I., Le Van Quyen, M., Gozlan, H., and Ben-Ari, Y. (2005). Epileptogenic actions of GABA and fast oscillations in the developing hippocampus. Neuron 48, 787–796.

Khosravani, H., Pinnegar, C.R., Mitchell, J.R., Bardakjian, B.L., Federico, P., and Carlen, P.L. (2005). Increased high-frequency oscillations precede in vitro low-Mg seizures. Epilepsia 46, 1188–1197.

Kilb, W., and Luhmann, H.J. (2003). Carbachol-induced network oscillations in the intact cerebral cortex of the newborn rat. Cereb. Cortex 13, 409–421.

Ko¨ hling, R., Vreugdenhil, M., Bracci, E., and Jefferys, J.G. (2000). Ictal epileptiform activity is facilitated by hippocampal GABAA receptor-mediated oscillations. J. Neurosci. 20, 6820–6829.

Lombroso, C.T. (2007). Neonatal seizures: gaps between the laboratory and the clinic. Epilepsia 48 (Suppl 2), 83–106.

Michelson, H.B., and Wong, R.K. (1991). Excitatory synaptic responses mediated by GABAA receptors in the hippocampus. Science 253, 1420–1423.

Oliva, A.A., Jr., Jiang, M., Lam, T., Smith, K.L., and Swann, J.W. (2000). Novel hippocampal interneuronal subtypes identified using transgenic mice that express green fluorescent protein in GABAergic interneurons. J. Neurosci. 20, 3354–3368.

Picardo, M.A., Guigue, P., Bonifazi, P., Batista-Brito, R., Allene, C., Ribas, A., Fishell, G., Baude, A., and Cossart, R. (2011). Pioneer GABA cells comprise a subpopulation of hub neurons in the developing hippocampus. Neuron 71, 695–709.

Quilichini, P.P., Diabira, D., Chiron, C., Ben-Ari, Y., and Gozlan, H. (2002). Persistent epileptiform activity induced by low Mg2+ in intact immature brain structures. Eur. J. Neurosci. 16, 850–860.

Ruusuvuori, E., Li, H., Huttu, K., Palva, J.M., Smirnov, S., Rivera, C., Kaila, K., and Voipio, J. (2004). Carbonic anhydrase isoform VII acts as a molecular switch in the development of synchronous gamma-frequency firing of hippocampal CA1 pyramidal cells. J. Neurosci. 24, 2699–2707.

Steriade, M., and Demetrescu, M. (1966). Post-primary cortical responses to flashes and their specific potentiation by steady light. Electroencephalogr. Clin. Neurophysiol. 20, 576–590.

Takács, V.T., Freund, T.F., and Gulyás, A.I. (2008). Types and synaptic connections of hippocampal inhibitory neurons reciprocally connected with the medial septum. Eur. J. Neurosci. 28, 148–164.

Tort, A.B., Rotstein, H.G., Dugladze, T., Gloveli, T., and Kopell, N.J. (2007). On the formation of gamma-coherent cell assemblies by oriens lacunosummoleculare interneurons in the hippocampus. Proc. Natl. Acad. Sci. USA 104, 13490–13495.

Traub, R.D., Spruston, N., Soltesz, I., Konnerth, A., Whittington, M.A., and Jefferys, G.R. (1998). Gamma-frequency oscillations: a neuronal population phenomenon, regulated by synaptic and intrinsic cellular processes, and inducing synaptic plasticity. Prog. Neurobiol. 55, 563–575.

Traub, R.D., Kopell, N., Bibbig, A., Buhl, E.H., LeBeau, F.E., and Whittington, M.A. (2001). Gap junctions between interneuron dendrites can enhance synchrony of gamma oscillations in distributed networks. J. Neurosci. 21, 9478–9486.

Traub, R.D., Draguhn, A., Whittington, M.A., Baldeweg, T., Bibbig, A., Buhl, E.H., and Schmitz, D. (2002). Axonal gap junctions between principal neurons: a novel source of network oscillations, and perhaps epileptogenesis. Rev. Neurosci. 13, 1–30.

Whittington, M.A., and Traub, R.D. (2003). Interneuron diversity series: inhibitory interneurons and network oscillations in vitro. Trends Neurosci. 26, 676–682.

Worrell, G.A., Parish, L., Cranstoun, S.D., Jonas, R., Baltuch, G., and Litt, B. (2004). High-frequency oscillations and seizure generation in neocortical epilepsy. Brain 127, 1496–1506.

SUPPLEMENTAL INFORMATION

Supplemental Data

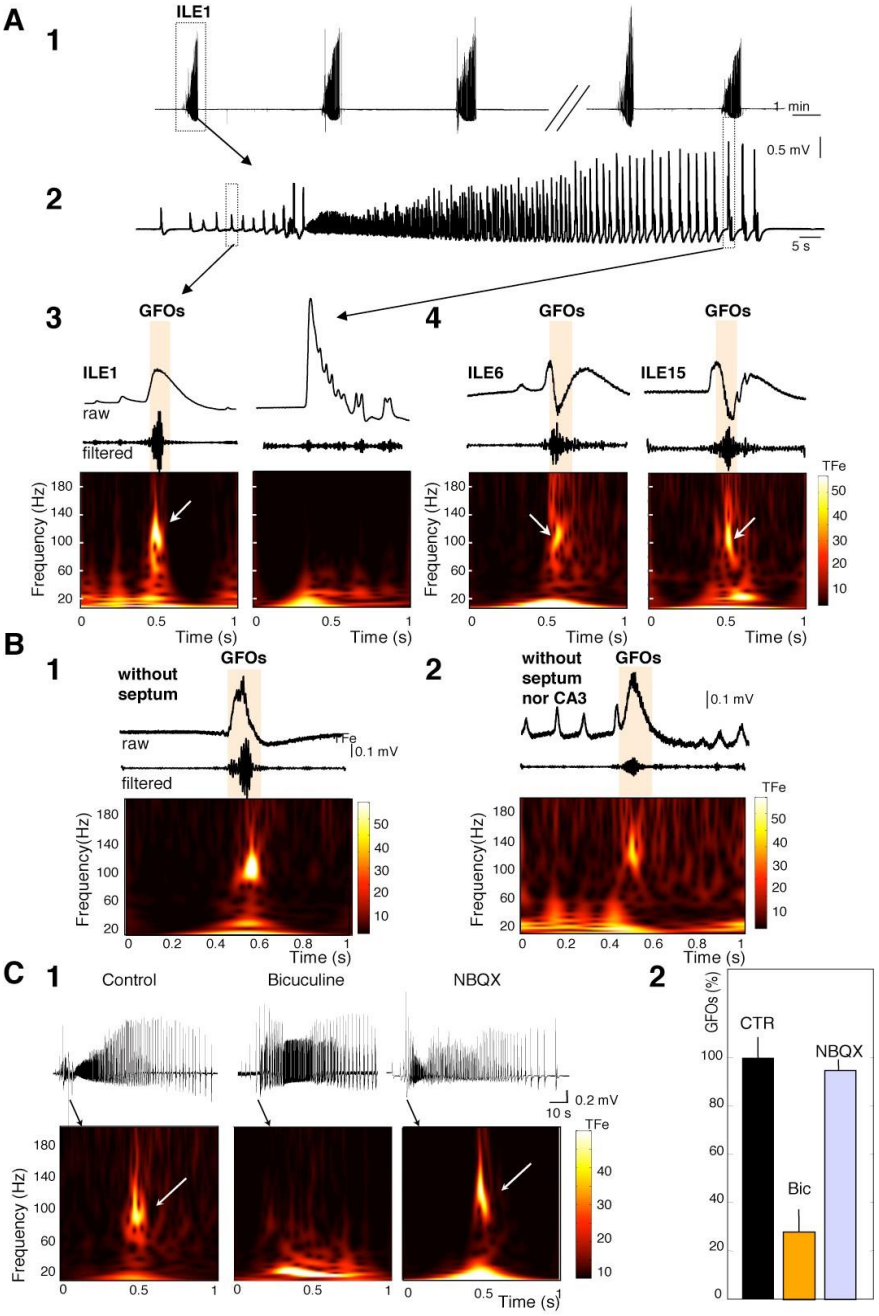

Figure S1. The CA1 region contains the sufficient circuitry to generate stable fast oscillations, which depend upon GABAA receptors activation.

(A1) Large network discharges (ictal-like activities; ILEs) started to occur twenty minutes following the perfusion of low Mg^{2+}-containing ACSF and showed a stable frequency (every six minutes) during long-term (> 2 h) recordings, as reported previously (Quilichini et al., 2002).

(A2) The first ILE is shown on an expanded time-scale.

(A3) Time-frequency (TF) content analysis revealed the presence of GFOs at ILE onset (ILE1). GFOs were specific to ILEs onset, as they were not present elsewhere during or between ILEs, including during isolated interictal-like events. (TFe: TF energy).

(A4) GFOs also displayed remarkable stability between the beginning and the end of the recording sessions. The GFOs at the onset of the 6th (ILE6) and 15th (ILE15) ILEs were very similar to the GFOs recorded at the onset of the first one.

(B1) Surgical removal of the septum did not affect the occurrence of GFOs in the CA1 region.

(B2) ILEs and GFOs were still present in the isolated CA1 region, demonstrating that this region retains the minimum circuitry to generate GFOs at ILE onset.

(C) The expression of GFOs was strongly reduced at ILE onset by the $GABA_A$ receptor antagonist bicuculline (10 µM; 24±6%, n=26 ILEs, $p<0.05$) but not by the AMPA/kainate receptor antagonist NBQX (10 µM; n=20 ILEs, $p>0.05$), indicating that GFOs depend upon $GABA_A$ receptor activation, not AMPA receptors. Neither the mean frequency (C1) nor the number (C2) of GFOs were affected by NBQX, suggesting that phasic AMPA/KA synaptic excitation by pyramidal cells is not required for their generation.

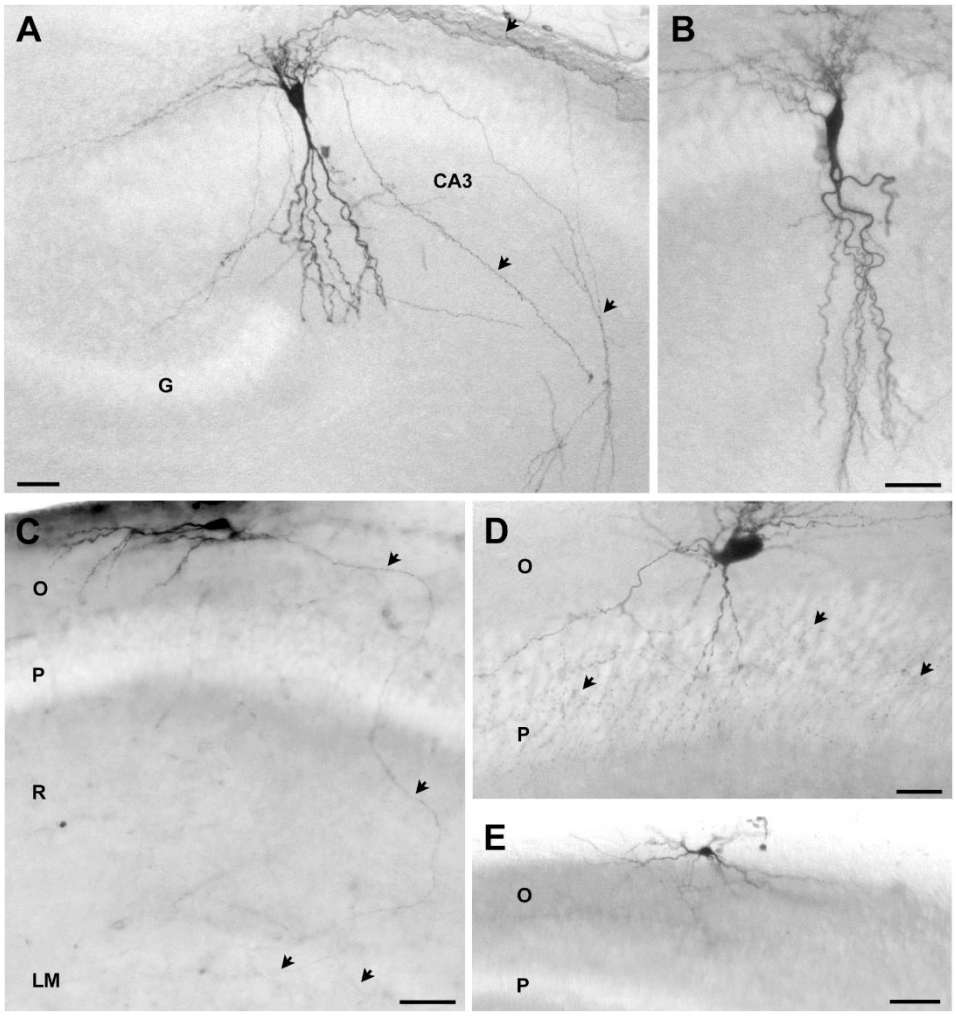

Figure S2. Examples of morphologically identified hippocampal neurons.

CA3 pyramidal cell recorded at P6. Arrowheads indicate the axon with its ramifications in CA1 (Schaffer collateral) and, locally, in CA3 (associational pathway).

CA1 pyramidal cell recorded at P5.

CA1 O-LM interneuron recorded at P5. Arrowheads indicate the axon with its ramifications in the stratum lacunosum moleculare.

CA1 stratum oriens perisomatic interneuron (putative basket cell) recorded at P6.

The axon (arrowheads) ramifies extensively in stratum pyramidale.

CA1 backprojecting interneuron recorded at P6.

Thirty-six biocytin labeled cells were identified as interneurons based on morphological features distinguishing them from pyramidal cells. Fourteen neurons could be assigned to a specific cell type. Incomplete axon filling of the remaining ones prevented a complete identification. This morphological analysis includes the neurons recorded in cell attached condition and voltage clamp during GFOs. A similar morphological analysis was performed following the experiments designed to determine the connectivity pattern of HS cells (see also Figure S3A-B), as well as the resting membrane potential and the chloride reversal potential in interneurons (see also Figure S3C-D).

O. stratum oriens, P: stratum pyramidale, R: stratum radiatum, LM: stratum lacunosum moleculare. Scale bars: A, B, C 50 μm; D 25 μm.

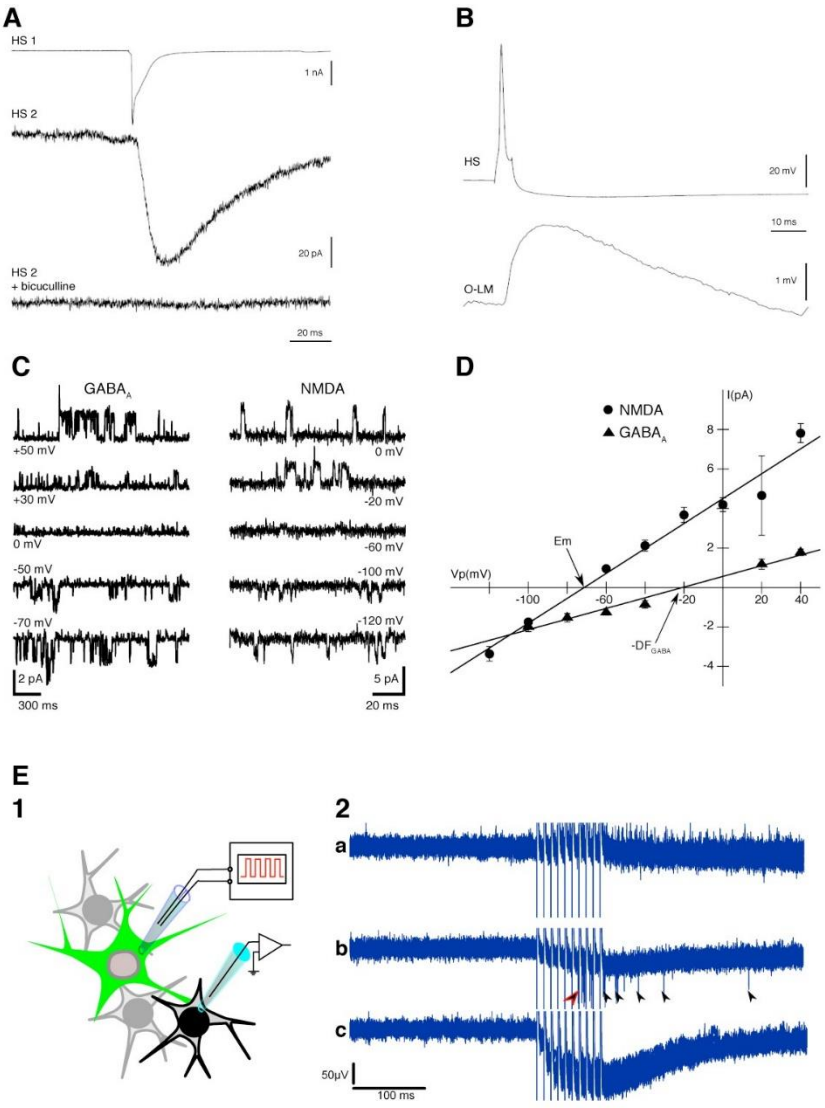

Figure S3. HS cells depolarize their targets.

A. Example of a connection between two HS cells (HS1 and HS2) recorded in voltage clamp mode using a CsCl based intracellular solution in normal ACSF. A 5 ms long depolarization to -40 mV of the HS1 triggered an unclamped action potential. The action potential triggered an IPSC in the postsynaptic HS2 cell. This IPSC was blocked following the application of the GABAA receptor antagonist bicuculline (10 µM).

Example of a connection between a HS cell and an O-LM interneuron recorded in current clamp mode using a K-gluconate based intracellular solution in normal ACSF. The HS and the O-LM cells were maintained at -60 mV and -80 mV, respectively. A 5 ms long, 400 pA current injection triggered an action potential in the HS cell, which produced a depolarizing IPSP in the postsynaptic O-LM interneuron. The neurotransmission was extremely reliable at these synapses. Each presynaptic cell was stimulated at least 100 times, for each connected pair. Neurotransmission failure was never encountered (not shown). The specific properties of these connections will be described in an independent study.

Examples of the cell-attached patch-clamp recordings of the GABAA (left panel) and NMDA (right panel) receptor channels at different holding potentials in low Mg2+ ACSF. (D) I-V relationships of the NMDA (circles) and GABAA (triangles) single channels permit to estimate resting membrane potential (Em) and the driving force of GABA mediated current (DFGABA) in low Mg2+ ACSF. The holding potential value (Vp) at which the IV curve of NMDA currents crosses the x-axis corresponds to the resting membrane potential. The cross point of the GABA IV-curve and the x-axis gives a negative value for DFGABA. In this example Em = -71.4mV, DFGABA = -21.1 mV. The reversal potential for GABA currents is thus -50.3 mV in this HS cell.

(E1) Schematic view of the experimental protocol: A large GFP+ interneuron (putative HS cell) was stimulated locally. Putative targets were probed with a second electrode using the loose cell configuration.

(E2) A train of 10 action potentials at 100 Hz was evoked in the presynaptic cell and the presence of spikes in the postsynaptic cell detected. (a) In normal ACSF, the stimulation did not evoke a spike in the target. (b) After 3 ILEs in low Mg2+ ACSF, the same stimulation protocol evoked spikes in the same postsynaptic cell. (c) The recording electrode was pulled back by 30 µm in low Mg2+. No spike was detected, showing that they were generated by the neuron in loose cell configuration.

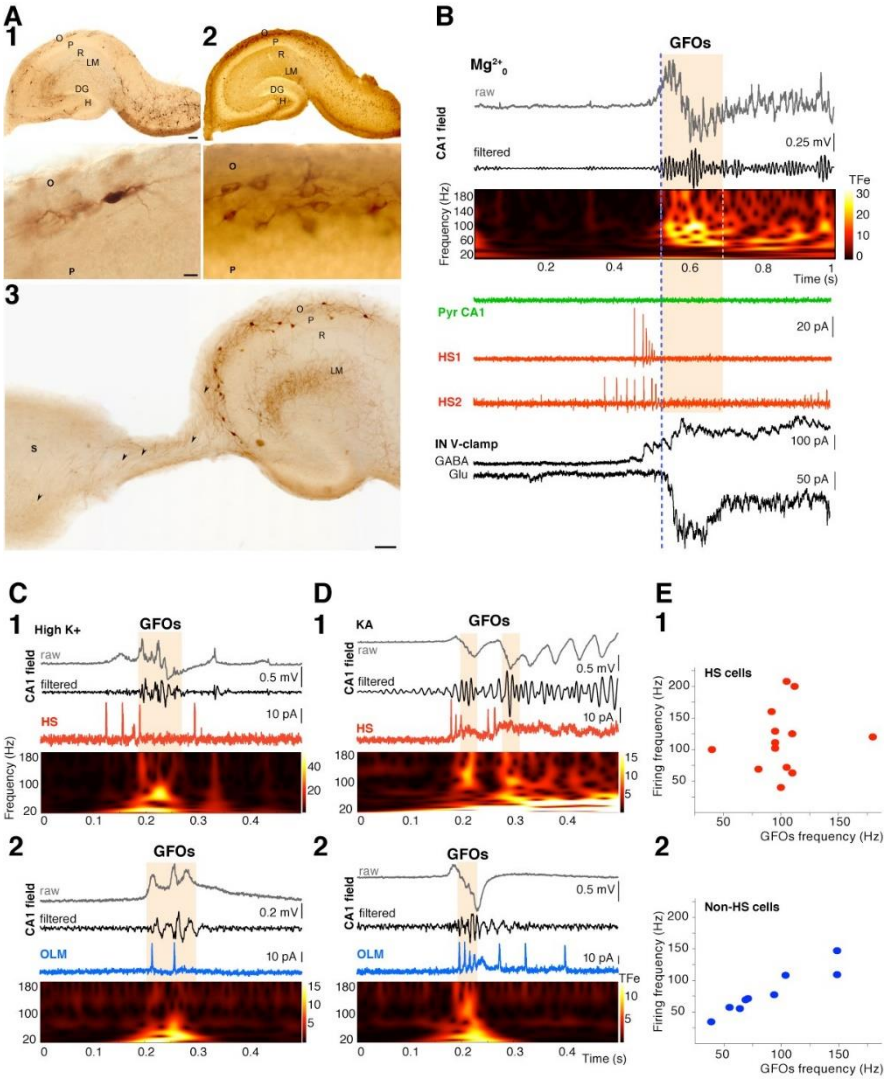

Figure S4. GFOs in GIN mice have similar properties to that found in rats. (A) Comparison of immunohistochemical labeling for GFP and somatostatin in adjacent sections of a GIN-mouse septo-hippocampal formation (SHF) at P6. The SHF was used for electrophysiological recordings (control illumination configuration) prior to immunohistochemical processing.

(A1) Some GFP-containing neurons are observed in the stratum oriens (O) of CA1-3. Top panel: Many neurons are present in the subiculum whereas only few are observed in the hilus (H) of the dentate gyrus (DG). Bottom panel: Higher magnification of CA1 stratum oriens showing one GFP-containing neuron with a horizontal dendritic arborization.

(A2) Numerous somatostatin-containing neurons are present in the stratum oriens of CA1-3 and in the subiculum. Top panel: Many neurons are also observed in the hilus of the dentate gyrus. Bottom panel: Higher magnification of the CA1 stratum oriens, showing that the number of somatostatin-containing neurons is about ten times higher than that of GFP-containing neurons in this region (compare bottom panels in A1 and A2). This result is similar to that found in adult GIN-mice, in which nearly 100% of GFPcontaining neurons in the hippocampal formation are GABAergic and contain somatostatin, whilst 15% of somatostatin-containing interneurons in the stratum oriens of CA1 contain GFP (Oliva et al., 2000).

(A3) Many GFP-containing neurons in the stratum oriens display morphological features of HS neurons.

Scale bars: A1-A2 top panels and A3 = 100 mm; A1-A2 bottom panels = 25 mm.

O. stratum oriens, P: stratum pyramidale, R: stratum radiatum, LM: stratum lacunosum moleculare.

Under low Mg2+ conditions, ILEs and GFOs recorded in GIN mice SHFs were similar to those recorded in rats and in normal mice. GFOs were present at the onset of the ILE. The CA1 pyramidal cell (Pyr CA1) remained silent, whilst simultaneously recorded HS neurons (HS1 and HS2) fired at high frequency before the occurrence of field GFOs. Two interneurons were simultaneously recorded in voltage-clamp mode in a different experiment (IN V-clamp). The traces were aligned of the field GFOs (not shown). GABAergic inputs, displaying a gradual build-up, arrived before field GFOs, consistent with the early firing of HS neurons. Glutamatergic inputs arrived after the initiation of the GFOs. Similar results were found in 5 CA1 pyramidal cells (n = 5, all silent), HS neurons (n=23) and interneurons (n=34).

Under high K+ conditions, ILEs and GFOs recorded in GIN mice SHFs were similar to those recorded in rats and in GIN mice. GFOs were present at the onset of the ILE (top panel): (C1) The HS neurons fired at high frequency before the occurrence of the GFOs (n=7) whereas (C2) the O-LM interneuron fired during the GFOs (n=4).

Triggered with kainic acid, ILEs and GFOs recorded in GIN mice SHFs were also similar. GFOs were present at the onset of the ILE (top panel): (D1) The HS cells fired at high frequency before the occurrence of GFOs (n=4) and (D2) the O-LM interneuron fired during GFOs (n=4 interneurons). Similar findings were obtained with 4AP (n=3, not shown).

E. Relationship between HS (E1) and non-HS (E2) neurons firing frequency and GFOs frequency in kainic acid, 4AP or high K+ conditions. The firing frequency of non-HS GABAergic neurons during GFOs is similar to the field GFO frequency. In contrast, the firing rate of HS cells before GFOs is on average higher than the GFOs mean frequency.

Supplemental Experimental Procedures

The intact septo-hippocampal formation (SHF)

All protocols were designed according to Inserm guidelines for the care and use of animals. Experiments were performed on intact SHFs taken from Wistar rats between postnatal day (day of birth) P5 and P7. Animals were killed and brains were extracted from the skull at 4°C. The two hemispheres were separated and dissected in order to obtain SHFs. They contained the hippocampal formation, the septum and parts of adjacent neocortical areas. The same procedure was applied for the experiments performed in GIN (GFP-expressing Inhibitory Neurons) mice intact SHFs. Each SHF was placed in oxygenated (95% O_2 and 5% CO_2) ACSF with the following composition (in mM): NaCl, 126; KCl, 3.5; $CaCl_2$, 2; $MgCl_2$, 1.3; $NaHCO_3$, 25; $NaHPO_4$, 1.2; glucose 10 (pH 7.3). After at least 1 h rest at room temperature, SHFs were transferred to the recording chamber where they were fully submerged and superfused with ACSF oxygenated at 32.0 ± 0.5°C at a flow rate of 7.0±0.2 mL/min. After 30 min, SHFs were then superfused with an ACSF without magnesium ions (low Mg ACSF). For some experiments (see Figure S4C-D), the epileptiform activity was generated by the addition of 300 nM of Kanic Acid in the ACSF or by the addition of 5mM of KCl in the ACSF.

Electrophysiological recordings

Field recordings were performed with extracellular microelectrodes filled with ACSF, usually placed in the *stratum oriens* of the CA1 area of the hippocampus. Simultaneously with field recordings, individual cells were recorded using patch-clamp techniques in cell-attached and whole-cell configurations. Interneurons and pyramidal cells were blindly recorded, or were identified using IR-DIC microscopy or a combination of fluorescence/IR-DIC for GIN mice through a 60x water immersion objective. Microelectrodes had a resistance of 4–8 MΩ, and internal solution of the following composition was used to record EPSCs and IPSCs (in mM): 135 Cs-gluconate, 2 $MgCl_2$, 0.1 $CaCl_2$, 1 EGTA, 2 MgATP, 0.5 Na_4GTP, 10 HEPES, 0.5% biocytin (pH 7.3; 270-280 mOsm). Access resistance was monitored throughout the experiments (range 12-30 MΩ). Experiments were discarded if series resistance increased by more than 20%. Cells were kept at -60 mV or +10 mV for the analysis of glutamatergic (NMDA and AMPA receptor-mediated currents) or GABAergic spontaneous postsynaptic currents, respectively. These currents were blocked by D-APV/NBQX and bicuculline, antagonists of NMDA/AMPA and $GABA_A$ receptors respectively (not shown). All data were acquired using an analogic-digital converter (Digidata 1322B Axon Instruments, CA, USA) and analyzed using Clampfit (Axon laboratories, CA, USA) or Matlab based software. During recordings, all neurons were passively filled with biocytin for *post hoc* morphological identification.

Measurement of membrane potential and reversal potential of $GABA_A$ receptormediated currents

Procedures are previously described in (Tyzio et al., 2003). Interneurons were first recorded in the cell-attached configuration, with a pipette solution containing nominally Mg^{2+}-free ACSF with NMDA (10 µm), glycine (1 µm), strychnine (1 µm) and biocytin (0.5%). The holding potential was varied to obtain IV curves of single NMDA channels. The potential at which NMDA receptor-mediated currents reverse corresponds to the cell resting membrane potential. The pipette was then gently removed and the same neuron re-patched in the cell configuration using an internal solution of the following composition (in mM): NaCl, 120; tetraethylammonium–Cl, 20; KCl, 5; 4-aminopyridine; 5; $CaCl_2$, 0.1; $MgCl_2$, 10; glucose, 10; GABA, 0.005; Hepes–NaOH, 10; 0.5% biocytin (pH 7.3). The holding potential was varied to obtain IV curves of single $GABA_A$ receptor-mediated currents and to define the reversal potential of $GABA_A$ receptor-mediated currents. At the end of the recording, the patch was ruptured to allow biocytin to diffuse during 20 min to enable *post hoc* morphological identification of the recorded interneurons.

Connected interneuron pairs

To test for synaptic connections between neuron pairs recorded in voltage clamp mode with the Cs-gluconate based internal solution described above, one cell was briefly (5 ms) depolarized to -40 mV to produce a voltage-escape action potential. The synaptic connection was assessed by the presence of a postsynaptic current in the second cell with a fixed latency, paired pulse depression/facilitation, a reversal potential in keeping with the composition of the

intracellular solution (-60 mV for GABAergic currents), and its sensitivity to the $GABA_A$ receptor antagonist bicuculline (10 μM).

To establish the connectivity pattern of HS cells, the internal solution of the following compositions were used (in mM): 150 CsCl, 4.6 $MgCl_2$, 0.1 Cal_2, 1 EGTA, 10 HEPES, 4 Na-ATP, 0.4 Na-GTP, 0.5% biocytin, pH 7.3, osmoloratity 260-290 mOsm (for voltage clamp recordings); and 90 K-gluconate, 40 CsCl, 1.2 NaCl, 3.5 KCl, 1.7 $MgCl_2$, 0.05 EGTA, 10 HEPES, 2 Na-ATP, 0.4 Na-GTP, 10 creatine-phosphate, 0.5% biocytin, pH 7.3, osmoloratity 260-290 mOsm (for current clamp recordings). The holding potential was kept at -60 mV in voltage clamp mode (CsCl based solution), giving rise to inward GABAergic currents in the postsynaptic cells. Presynaptic cells were voltageclamped at -60 mV, and unclamped action potentials were triggered by 5 ms depolarizations to -20 mV. In current-clamp mode (K-gluconate based solution), the membrane potential of the postsynaptic cell was kept at -80 mV with constant current injection, giving rise to depolarizing GABAergic postsynaptic potentials. The presynaptic cell was kept at -60 mV and injecting 5 ms depolarizing pulses (400-600 pA) evoked action potentials. Presynaptic interneurons were stimulated every 8 s. Prior recordings, cells with a large multipolar soma close to the *stratum oriens* surface were selected under visual control. This selection procedure led to 1/3 probability to find a synaptic connection between two cells.

Pharmacological experiments

They were performed as previously described (Quilichini et al., 2002). Briefly, after the induction of 3 network discharges, the drug solution was applied for 30-60 min. GFOs were determined (see below) at the onset of the 3 initial ILEs (control) and at the onset of ILEs occurring during drug application.

Histochemical Methods

All SHFs processed for the detection of biocytin-filled neurons or for the green fluorescent Protein (GFP) and somatostatin immunohistochemical labeling were fixed immediately after electrophysiological recordings in a solution of 4% paraformaldehyde in 0.12 M phosphate buffer (PB, pH 7.4) overnight at 4°C. After fixation they were rinsed in PB for 1.5 hr, cryoprotected in a 20 % sucrose solution overnight at 4°C and quickly freeze-thaw in liquid nitrogen. SHFs were cut in a transverse plane on a vibratome and 150 μm thick sections were collected sequentially in PB.

Detection of biocytin-filled neurons was performed for each SHF, processing all adjacent sections collected from the whole structures as followed. Sections were pretreated for 30 min in 1% H_2O_2 prepared in PB to neutralize endogenous peroxidases, rinsed in a potassium phosphate-buffered saline (0.02 M KPBS, pH 7.4) and incubated overnight in 1:100 avidin-biotinylated horseradish peroxidase complex (Vestastain ABC Peroxidase kit, Vector laboratories, Burlingame, CA) diluted in KPBS containing 0.3 % Triton X-100. After 1 hr rinses in KPBS, sections were then processed for 15 min with 0.06% 3,3'-diaminobenzidine tetrahydrochloride (DAB, Sigma, France) and 0.01% H_2O_2 diluted in KPBS, rinsed in KPBS, mounted on Superfrost plus slides and cover-slipped in an aqueous mounting medium (Crystal/Mount, Biomeda, Foster City, CA). Biocytinlabeled interneurons were identified and their complete dendritic and axonal arborisations were reconstructed from serial adjacent sections with the NeuroLucida system (Microbrightfield, Colchester, VT).

Immunohistochemical labeling for GFP and somatostatin was performed in 8 SHFs. For each SHF, two adjacent sections, every three sections, were selected through the entire structures. One section was processed for the immunodetection of GFP, the other one for the detection of somatostatin as followed. Sections were pretreated for 30 min in 1% H_2O_2 prepared in PB to neutralize endogenous peroxidases and rinsed for 1.5 hr in 0.02 M KPBS. Then, sections were pre-incubated for 1 hour at room temperature (RT) in KPBS containing 0.3% Triton X-100, 3% normal goat serum (NGS, Vector) and incubated overnight at RT in a polyclonal antiserum directed against GFP (rabbit anti-GFP, IgG fraction, A11122; Molecular Probes, Eugene, OR; 1:3000) or a polyclonal somatostatin-antiserum raised in rabbit (IHC 8001, Peninsula Laboratories, Belmont, CA; 1:4000) diluted in KPBS containing 0.3% Triton X-100, 1% NGS. After these steps, sections were rinsed in KPBS, incubated for 1 hr at RT in biotinylated goat anti-rabbit immunoglobulin G (Vector) diluted 1:200 in KPBS containing 3% NGS; rinsed in the same buffer and incubated for 1 hour at RT with avidin-biotinylated horseradish peroxidase complex (Vector) diluted 1:100 in KPBS. After 1 hr rinses in KPBS, sections were processed for 15 min with 0.06% 3,3'-diaminobenzidine tetrahydrochloride (DAB, Sigma, France) and 0.01% H_2O_2 diluted in KPBS. The sections were then rinsed in KPBS, mounted on Superfrost plus slides, dried, dehydrated, and coverslipped with permount (Fisher Scientific, Washington, PA).

Drugs

Bicuculline methochloride, 2,3-dioxo-6-nitro-1,2,3,4-tetrahydrobenzo[f] quinoxaline-7sulfonamide (NBQX) and kanic acid were purchased from Tocris Cookson Ltd (UK). Drugs were first dissolved in water or in DMSO and then diluted in ACSF. The final concentration of 0.1% DMSO has no effect on network activity.

Gamma-frequency oscillations analysis

A wavelet time-frequency (TF) analysis was used to analyze to determine precisely the mean frequency, the beginning and the duration of the field GFOs. The advantage of the wavelet analysis lies in the fact that the time resolution is variable with frequency, so that high frequencies have a sharper time resolution (Le Van Quyen and Bragin, 2007; Torrence and Compo, 1998). The Gabor wavelet is applied and uses a wave-like scalable function that is well localized in both time and frequency:

$$\Psi_{\tau,f}(u) = \sqrt{f}\,\exp(\,j2\pi f\,(u-\tau))\,\exp\left(-\frac{(u-\tau)^2}{\sigma^2}\right).$$

This wavelet represents the product of a sinusoidal wave at frequency *f*, with a Gaussian function centered at time t, with a standard deviation s proportional to the inverse of *f*. The wavelet coefficients of a signal *x(t)* as a function of time (t) and frequency (f) are defined as: $W(\tau, f) = \int_{-\infty}^{+\infty} x(u)\Psi_{\tau,f}(u)du$. It depends solely on s, which sets the number of cycles of the wavelet: *nco*= 6fs. This value *nco* determines the frequency resolution of the analysis by setting the width of the frequency interval for which phase are measured. We chose *nco=5*.

As a criterion of the significance for the TF representations, we required that the TF peak energy to exceed the mean + 3 standard deviation of a baseline taken far away from synchronized events. Thus, by using the background signal in the same way at each frequency, the method allowed to statistically control the levels of oscillatory activity from that one would expect by chance and fairly compare oscillatory episodes across frequencies. To detect oscillatory events, we designed an algorithm to identify the periods within the signal that exhibits high-power oscillatory activity at a particular frequency, lasting a few cycles. We defined oscillatory events by detecting local maxima in the normalized TF representations with duration longer than *K* cycles at a particular frequency, during which the power exceeded *N* standard deviations of baseline. We have adjusted the thresholds (*K*,*N*) to be relatively insensitive to sharp transients. The duration threshold was set to 5 cycles (i.e. *5/f* sec) and the amplitude threshold was set to 3 standard deviations.

Phase-locking between two field oscillations

We used the procedure described in (Lachaux et al., 1999) to overcome some limitations of conventional methods which cannot disentangle instantaneous amplitudes and phases (see (Le Van Quyen et al., 2001) for details). The important advantage of this method is that the phase components can be analyzed separately from the amplitude components, which can be quite noisy or even non-correlated (Le Van Quyen and Bragin, 2007). Two steps are used: 1) *Estimation of the phase*: The first step is to measure the instantaneous phase-difference between signals around the frequency of interest. The phase of the signals are extracted from the coefficients of their wavelet transform at the target frequency between 60 and 200 Hz. These coefficients are the result of a convolution of the original signal with a complex Gabor wavelet (see previous section). 2) *Quantification of the degree of phase locking*: The phase-difference between the signals x and y at frequency f and time t can be derived from the angles of their wavelet-coefficients:

$$\exp(\ j(\phi_y(f,\tau) - \phi_x(f,\tau))) = \frac{W_x(\tau,f)W^*y(\tau,f)}{|W_x(\tau,f)||W_y(\tau,f)|}$$

A phase Locking value (PLV) is then defined as:

$$PLV\ (f,t) = \left| \frac{1}{\delta} \int_{t-\delta/2}^{t+\delta/2} \exp(\ j(\phi_y(f,\tau) - \phi_x(f,\tau)))\, d\tau \right|$$

PLV depends then on two parameters: *nco* (see previous section) and the size d of the window of temporal integration, which can be expressed in a number of cycles at a chosen frequency *f*: *ncy* = *f*.d. In this sense, *ncy* determines the temporal resolution of the analysis where the synchrony estimation remains stable. We usually chose *ncy* between 6 and 10. PLV ranges from 0 to 1 with 1 indicating the strongest phase-locking. The significance of each PLV is estimated via a comparison with a distribution PLV obtained between independent Gaussian signals (100 pairs) with same duration as the original signals are generated. For each of them, the maximum PLV is measured to build a distribution of 100 values. A significant synchrony is detected when less than 1% of the surrogate values were greater than the original PLV (Le Van Quyen et al., 2001).

Phase-locking between spikes and field oscillations

We used the procedure described in (Jacobs et al., 2007) which characterizes the phase distribution of the field oscillations at the moment of the spike onset. If the firing of a given neuron is independent of the field oscillation, the distribution of its phase values will be random. Conversely, if the firing of a given neuron is phase-locked to the field oscillation, its phase value distribution will be unimodal. Following this strategy, oscillatory phase and power of the field potential was computed using Gabor wavelets (*nco=5*) at frequencies between 20 and 200 Hz (see previous paragraphs). We considered a neuron phase-locked at a particular frequency if the hypothesis of circular uniformity for its field phase distribution could be rejected at $P < 0.001$ using a Bonferroni-corrected Rayleigh test (Fisher, 1993). Briefly, given *n* phase values f_i define the first trigonometric moment $m = (1/n)\sum_1^n e^{j\phi_i}$. The sample mean direction or preferred phase μ is given by the orientation of *m*, while the mean resultant value R is given by the modulus of *m*. The Rayleigh statistic is $Z = n R^2$, and the probability that the null hypothesis of sample uniformity holds is given by $P = e^{-Z}[1 + (2Z - Z^2)/(4n) - (24Z - 132Z^2 + 76Z^3 - 9Z^4)/(288n^2)]$. For $n > 50$, the approximation $P = e^{-Z}$ is adequate (Fisher, 1993; Siapas et al., 2005).

Instantaneous frequency of spike and post-synaptic current

Spikes were detected in cell-attached recordings using a threshold detection algorithm (>4:1 signal to noise ratio). The instantaneous spike frequency was measured by convolving the timing of each detected event with a Gaussian function of variable standard deviation (Szucs, 1998). Post-synaptic current (PSC) were counted individually in whole-cell recordings if their peak height was greater than the half-peak amplitude of the background activity. The instantaneous PSC frequency was measured by convolving the timing of each detected event with a Gaussian function of a standard deviation of 10 ms.

Ablation of GFP-containing interneurons

After recording several GFOs in GIN mice, the region around the recording electrode was scanned under visual control and florescence illumination, until a GFP

interneuron in *stratum oriens* close to the surface (where most HS cells are located) was found. The region remained illuminated during 5 min. Under a 60x Olympus objective on a Zeiss FSII microscope and with maximum power illumination (Zeiss), this duration was found to be optimal for all fluorescence to disappear in the field. Before the continuous illumination, the soma of GFP-containing (fluorescent) neurons was also easily identifiable under IR. Following focused illumination, the soma was no longer observed (neither the nucleus, nor a "phantom cell" could be seen), neither under fluorescence illumination nor IR. However, GFP-negative interneurons could still be visible under IR in the illuminated field (not shown). Over-activation of GFP is deleterious, presumably via the production of free radicals. In these preparations, no biocytin-filled GFP-positive neurons (n=5, recorded before illumination) were ever detected. However, in two SHFs, biocytin-filled axonal processes were observed in the septum, strongly suggesting that HS cells (n=2) were recorded and labeled before the illumination protocol (not shown). After checking the disappearance of the illuminated GFP-positive neurons, the field was moved to the next target GFP-positive neurons. The field was moved in an elongated spiral-like manner, centered on the extracellular recording electrode, with a predominant direction along the long, septo-temporal, axis of the hippocampus. In parallel to the illumination procedure, the presence of GFOs was checked online each time ILEs occurred. The illumination procedure was stopped when 3 successive ILEs did not display GFOs at their onset. Sham experiments were performed the contralateral SHFs recorded in the same conditions either illuminated and scanned under visible light with the 60X objective (n=3) or illuminated with fluorescence with a wide field 5X Zeiss objective (n=3). Sham illumination lasted one hour, exceeding by 15 min the longest duration of the focused illumination procedure. Immunohistochemical experiments for the detection of GFP were then performed in these preparations to assess the loss of GFP-immunolabeled neurons in the regions directly under illumination, or their survival in control experiments.

Elimination of GFP-negative interneurons in GIN mice

In order to destroy GFP-negative *stratum oriens* interneurons, we designed a doublebarreled ACSF shotgun. Electrodes made of theta tubes were pulled with the parameters used for patch clamp electrodes. Both compartments were filled with ACSF. The electrode was inserted in a modified electrode holder. Two wires were introduced in each compartment, and connected to a stimulator. *Stratum oriens* GFP-negative interneurons were selected around the field electrode. The tips of the double-barreled electrode were apposed to the soma of the interneuron. The stimulus pulse ejected a "bullet" of ACSF (at an estimated maximum distance of 5 µm), which perforated the membrane, effectively killing the interneuron. The procedure was repeated by moving around the stimulating electrode. This type of stimulation was not sufficient to evoke a field response.

HS cells stimulation experiments

Putative HS cells were identified as GFP-positive neurons with large cell body located in the *stratum oriens*. The HS cell was stimulated with bipolar glass electrode 5-10mkm tip diameter pulled from theta glass tube (Warner instruments). To check the stimulation effectiveness, 200 µs (1/5s) stimuli were applied and a response of the stimulated neuron was recorded with a recording glass electrode (5-8 µm tip diameter) connected to the preamplifier of the Multiclamp 700b (current clamp mode). We used the loose patch configuration to test the result of the HS cell stimulation on neighboring neurons. To establish a contact with the target neuron, the recording electrode was approached to the cell body and a gentle suction was applied. The stimulus current intensity was adjusted to the minimal value sufficient to induce spiking in the stimulated neuron (50170µA). Then 2-4 neurons surrounding stimulated one were tested for their ability to generate spikes in response to the high frequency stimulation (10 stimuli of 100Hz train) of the putative HS cell (Figure S3E1). Before ILEs induction, spikes never occurred in the 500ms time window after the stimulation onset (Figure S3E2a). After transition to low Mg^{2+} ACSF and the occurrence of 3 ILEs, the response on stimulation of the GFPpositive neuron was recorded in same neurons. To check that the detected spikes are indeed generated by the recorded cell, the stimulation was repeated after the recording electrode had been taken ~30 µm away from the recorded cell. As Figure S3E2c shows, no spike was detected in such configuration.

Supplemental references

Fisher, N. (1993). Statistical analysis of circular data (Cambridge: Cambridge University Press).

Jacobs, J., Kahana, M.J., Ekstrom, A.D., and Fried, I. (2007). Brain oscillations control timing of single-neuron activity in humans. J Neurosci *27*, 3839-3844.

Lachaux, J.P., Rodriguez, E., Martinerie, J., and Varela, F.J. (1999). Measuring phase synchrony in brain signals. Hum Brain Mapp *8*, 194-208.

Le Van Quyen, M., and Bragin, A. (2007). Analysis of dynamic brain oscillations: methodological advances. Trends Neurosci *30*, 365-373.

Le Van Quyen, M., Foucher, J., Lachaux, J., Rodriguez, E., Lutz, A., Martinerie, J., and Varela, F.J. (2001). Comparison of Hilbert transform and wavelet methods for the analysis of neuronal synchrony. J Neurosci Methods *111*, 83-98.

Oliva, A.A., Jr., Jiang, M., Lam, T., Smith, K.L., and Swann, J.W. (2000). Novel hippocampal interneuronal subtypes identified using transgenic mice that express green fluorescent protein in GABAergic interneurons. J Neurosci *20*, 3354-3368.

Quilichini, P.P., Diabira, D., Chiron, C., Ben Ari, Y., and Gozlan, H. (2002). Persistent epileptiform activity induced by low Mg2+ in intact immature brain structures. Eur.J Neurosci. *16*, 850-860.

Siapas, A.G., Lubenov, E.V., and Wilson, M.A. (2005). Prefrontal phase locking to hippocampal theta oscillations. Neuron *46*, 141-151.

Szucs, A. (1998). Applications of the spike density function in analysis of neuronal firing patterns. J Neurosci Methods *81*, 159-167.
Torrence, C., and Compo, G.P. (1998). A practical guide to wavelet analysis. Bulletin of the American Meteorological Society *79*, 61-78.
Tyzio, R., Ivanov, A., Bernard, C., Holmes, G.L., Ben Ari, Y., and Khazipov, R. (2003).
Membrane potential of CA3 hippocampal pyramidal cells during postnatal development. Journal of Neurophysiology *90*, 2964-2972.